Body-to-Body Channel Characterization and Modeling Inside an Underground Mine

Moulay El Hassan El Azhari, Larbi Talbi, *Senior Member, IEEE*, and Mourad Nedil, *Senior Member, IEEE*

***Abstract*— In this article, the use of circularly polarized multiple-input–multiple-output (MIMO) antenna systems is proposed as a new solution for future body-to-body (B2B) applications. Four B2B channels have been characterized inside a mine. The statistical parameters of the B2B channels using co-positioned (CP) and 90° rotated (90R) antennas have been determined. Path loss (PL) exponent values varied between 2.33 and 1.26. The time dispersion parameters and channel capacities are computed for both CP and 90R scenarios. Moreover, channel correlation matrices and the Rician K-factor have been determined and discussed in terms of their effect on capacity and root mean square (rms) delay spread. Overall, the circularly polarized setup exhibits the best performance in terms of PL, rms delay spread, and channel capacity. The nonline-of-sight (NLOS) situation caused a significant drop in channel capacity due to the significant increase in PL, and an increase in the rms delay spread due to the multipath richness. The MIMO-NLOS scenario exhibits the highest throughput gain of 1.752 (at an SNR of 20 dB), due to its low branch correlation. A model of the B2B impulse response has been created based on a statistical–empirical approach to determine the optimal path amplitudes and time of arrival.**

***Index Terms*— Body to body, channel capacity, frequency response, impulse response, multiple-input–multiple-output (MIMO), path loss (PL), polarization.**

I. Introduction

THE human body is considered as a challenging environment for the wireless communication systems. In fact, the wireless body area network (WBAN) channel is affected by the complex antenna–body electromagnetic interaction, the body movement, and the propagation characteristics of the local environment [1]. The characterization of the WBAN channel is of interest to an increasing number of research areas such as medical, military, sports, and recreational applications [1]. For instance, a WBAN deployed to the medical field may use sensors to monitor life vitals, such as heart rate and body temperature. Similarly, in the mining field, vital signs, acceleration, and proximity sensors (attached to the miners) could be used to improve the miners' safety and help coordinate mine rescue efforts, when an accident occurs.

Motivated by an increasing pressure to improve in-mine communication systems, numerous studies have focused on underground channel characterizations and modeling. Hence, characterization studies have reported the channel properties for different frequency bands, diversity configurations, and antenna selections under different environmental conditions [2]–[6]. Ben Mabrouk *et al.* [7] studied the effect of nonline-of-sight (NLOS) on the signal propagation at UWB using Vivaldi antennas for two different multiple-input–multiple-output (MIMO) configurations (parallel and 30° antenna set up, where the antenna planes form 30° angle). A general improvement of the channel parameters was observed for the 30° MIMO antennas compared to the parallel setup. With regard to beam forming techniques, the Butler matrix was investigated in [8] for underground mining uses at 2.4 GHz. The beam forming module was found to improve the average channel capacity of a MIMO multipath channel (compared to a conventional uniform linear array). Moreover, the effect of directivity on the 2.4 GHz underground RF channel is studied in [9] for a point-to-point system and in [10] and [11] for an off-body system. It was found that the monopole-MIMO channel capacity is better than that of the patch-MIMO setup in a mine environment for both point-to-point and off-body scenarios. The on-body channel in an underground mine for both static and dynamic topologies has also been studied [1]. The effectiveness of spatial diversity was confirmed for on-body channels at both static and dynamic scenarios.

With regard to WBAN channel models, Reusens *et al.* [12] presented a path loss (PL) model based on measurements of the static on-body channel for transmitting–receiving (Tx-Rx) separations of 5–40 cm. It is often easier to use statistical approaches to analyze RF channels in a nonuniform environment such as the WBAN channel [13]. In fact, the geometry of the human body allows a multitude of signal path trajectories of similar lengths but different propagation mechanisms. These include the line-of-sight (LOS), NLOS, and creeping wave scenarios, which greatly affect the signal propagation. Hence, it is difficult to fit a general distance-related PL model to the data obtained. Moreover, the peculiarity of the underground environment adds

Manuscript received February 26, 2019; revised October 7, 2019; accepted January 18, 2020. Date of publication February 3, 2020; date of current version June 2, 2020. This work was supported by the Natural Sciences and Engineering Research Council of Canada (NSERC). *(Corresponding author: Moulay El Hassan El Azhari.)*

Moulay El Hassan El Azhari is with the University of Quebec at Outaouais, Gatineau, QC J8X 3X7, Canada (e-mail: moulay.elazhari@uqat.ca).

Larbi Talbi is with the University of Quebec at Outaouais, Gatineau, QC J8X 3X7, Canada.

Mourad Nedil is with the School of Engineering, Université du Québec en Abitibi-Témiscamingue, Val-d'Or, QC J9P 1Y3, Canada.

Color versions of one or more of the figures in this article are available online at http://ieeexplore.ieee.org.

Digital Object Identifier 10.1109/TAP.2020.2969746

to the complexity of the WBAN channel and makes the received signal even more difficult to predict with reasonable accuracy [14]. Several approaches have been proposed to model PL for underground propagation channels. A Friis-based statistical model has been investigated in [9]–[11] to derive the PL exponent through the linear regression analysis of the PL results as a function of the logarithm of the distance. The dual-slope PL model is proposed in [15]. Other PL models use multiples break points (three or more) to separate the areas characterized by different PL exponents due to a major change in the geometry of the mine gallery [16]. The linear regression model seems suitable for WBAN studies because of its simplicity and accuracy, especially that propagation distances are generally small, compared to the point-to-point RF studies. Moreover, this model conveniently reveals crucial shadowing information [13].

As for the short-term fading channel models, which consist in developing a model for the impulse response, different models are presented in the works of literature, such as the two-ray model, the exponential model, and the Saleh–Valenzuela (S-V) channel model [13]–[17]. They were adopted for indoor environments with different levels of accuracy, which usually compromises simplicity. The S-V channel model is used when measurements indicate the presence of multiple clusters, while the two-ray model is rarely accurate [13]–[17]. The exponential model is known to be appropriate for indoor channels [17]. In underground mines, stochastic and empirical approaches have been experimented to model the path arrival, path amplitudes, and time of arrival [18]. These techniques avoid the complexity of deterministic models, which seems to be inaccurate in the presence of rough structures such as a mine [18]. However, they failed to present a complete impulse response channel model.

The design of an in-mine communication system requires careful choosing of the antenna characteristics. It is experimentally observed that the underground wireless communications suffer from some degree of depolarization due to the miners' movement and rough surface reflections [14]. Hence, the communication quality could be significantly improved through the use of circularly polarized antennas, which radiate energy in both the horizontal and vertical planes and exhibit low polarization mismatch losses [14]. In fact, the improvement in MIMO performance due to the use of circularly polarized antennas has been demonstrated in [19] and [20] in terms of diversity gain and system capacity.

This article experimentally characterizes the body-to-body (B2B) channel using circularly polarized antennas and compares the results to those of a linear patch antenna. This section aims to study the effect of circular polarization on the MIMO-B2B channel in a mine environment. Moreover, the effect of antenna misalignment and that of NLOS are also studied. The different considered scenarios are summarized in Table I.

In order to study the small-scale fading, the time dispersion parameters have been used and compared for both polarization scenarios. The channel capacity is then determined with two methods, namely at a constant SNR and at a fixed Tx power, to study the effect of multipath components (MPCs) and that of the PL, as explained in [21]. The multipath richness is quantified using the Rican K-factor. Moreover, the branch correlations are determined and used to explain the MIMO throughput gain. The noise floor was deduced empirically by visually inspecting a set of impulse responses; a chosen value of -80 dBm is higher than the vector network analyzer (VNA) sensitivity (-110 dBm) and the calculated thermal noise (about -114 dBm), which gives conservative SNR values. The large-scale results are analyzed in terms of PL, which has been modeled with a simple PL exponent model using linear regression analysis. An impulse response channel model has been developed through empirical and statistical approaches in order to characterize the B2B channel.

TABLE I
STUDIED SCENARIOS

Polarization	**Circular (Cir)**			**Linear (Lin)**
Scenario	CP-LOS	90R-LOS	CP-NLOS	CP-LOS

To the best of our knowledge, no B2B channel characterization and modeling study was performed for in-mine applications. The novelty of this article consists of four main contributions: First, the B2B channel characterization in a mine gallery is presented, for the first time. Second, the circular polarization is compared to the linear one for B2B applications. Third, the co-positioned (CP) antennas' scenario is compared to the 90° rotated (90R) antennas' one and LOS is compared to NLOS for the B2B channels. Fourth, a novel impulse response model based on statistical and empirical approaches was developed, which closely approximated a measurement-based channel impulse response.

This article is organized as follows. Section II describes the measurement procedure. Section III explains the experimental results. Finally, this article is concluded in Section IV.

II. MEASUREMENT PROCEDURE

A. Description of the Underground Mine

In a currently nonoperating gold mine, located in Val-d'Or city (in northern Quebec), a gallery at a depth of 90 m was used for the 2.4 GHz measurements. This gallery is characterized by very rough surfaces, humidity nearing 100%, temperature around 8 °C, and lots of dust particles. It stretches over a length of 20 m with a height of about 2.45 m and a width of approximately 5 m. Water puddles, mining machines, and ceiling implanted metal rods and nets are present along the gallery. This usual mine environment favors the multipath phenomenon due to reflection and diffraction from the rough surfaces.

B. Measurement Setup

Two MIMO antenna systems, namely a 2×2 MIMO circularly polarized (Cir) patch antenna system and a 2×2 MIMO linearly polarized (Lin) patch antenna system, are used

Fig. 1. Photograph of the mine gallery setup.

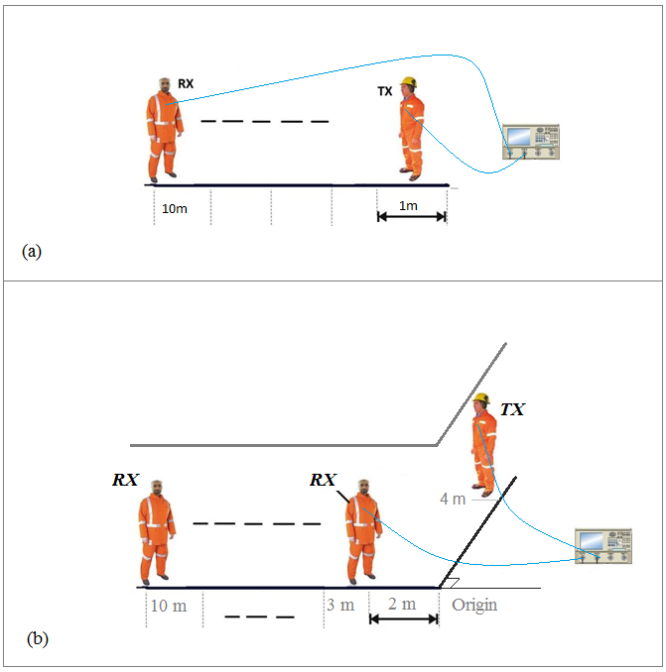

Fig. 2. Underground experiment setups for (a) LOS and (b) NLOS scenarios.

in the measurements. The polarization plane for the linear setup is vertical. The two antennas have a gain of 6.6 dBi and an axial ratio (AR) less than 3 dB at 2.4 GHz. The spatial diversity antenna separation is equal to half of the wavelength ($\lambda/2$). A VNA is used to measure the S parameters at the 2.3–2.5 GHz band. During the measurements, the Tx and Rx antennas were fixed on the chest of two students wearing a miner's outfit, as illustrated in Figs. 1 and 2. The Rx human subject was displacing at 1 m steps from a starting position of 1 m to a final distance of 10 m for the LOS measurements. In the NLOS scenario, the Rx and Tx human subjects were standing at two different mine tunnels, as shown in Figs. 1 and 2. The transmitter is positioned at 4 m distance from the origin and the receiver is positioned at different distances from the origin, starting from 2 m to a final distance of 10 m. In the postprocessing results, the NLOS distances are represented by the notation: 4m/xm, where xm is the distance (in meters) of Rx from the origin.

TABLE II
MEASUREMENT SYSTEM CONFIGURATIONS

Parameter	Value
Frequency	2.3–2.5 GHz
Bandwidth	200 MHz
Transmitting power	-10 dBm
Sweep points	2049
Noise floor	-80 dBm
Tx gain	6.6 dBi
Rx gain	6.6 dBi
Cable loss	0.6 dB/m
Antenna types	Linearly and circularly polarized patch
Antenna height	1.5 m
Human subjects' height	1.80 m

Ten snapshots (each with 2049 frequency points) were taken at each measurement position. The measurement parameters are described in Table II.

III. MEASUREMENT RESULTS

A. Channel Impulse Response

The S parameters were measured for the B2B-MIMO channel using a VNA; 2049 frequency points were considered at the 2.3–2.5 GHz band. In order to determine the impulse response (which characterizes this B2B-MIMO transmission channel), an inverse fast Fourier transform (IFFT) was applied to the MIMO transfer function (corresponding to the average of the measured S_{21} values over the number of snapshots and MIMO subchannels) using a hamming window. The hamming window is meant to correct for the IFFT-induced ripple in the delay domain (since the frequency response has a limited band).

Moreover, the power delay profile (PDP) (which gives the relative received power as a function of the excess delay) was determined from the impulse response as follows [7]:

$$\mathrm{PDP(t)} = \|h(n)\|^2 \tag{1}$$

where $\|\cdot\|$ is the modulus operation and $h(n)$ is the impulse response.

The effect of circular polarization and that of NLOS were considered. Specifically, the circular CP (Cir-CP) MIMO setup was compared to the circular-90° rotated (Cir-90R) MIMO setup. The Cir-CP was also compared to the linear-CP (Lin-CP) setup. Finally, the Cir-CP at LOS was compared to the Cir-CP at NLOS.

The normalized B2B-MIMO impulse responses for both circularly and linearly polarized patch antennas at CP and 90R scenarios, with LOS and NLOS topologies, are represented in Figs. 3 and 4.

From the above impulse responses, it is noticed that the Cir-MIMO-CP MPCs power content is similar to that of the Cir-MIMO-90R one. In fact, at LOS, both the Cir-MIMO-CP and the Cir-MIMO-90R exhibit low MPC powers and a significant deterministic power content. This is expected since the circularly polarized antenna is able to effectively receive signals at both horizontal and vertical directions; at the same

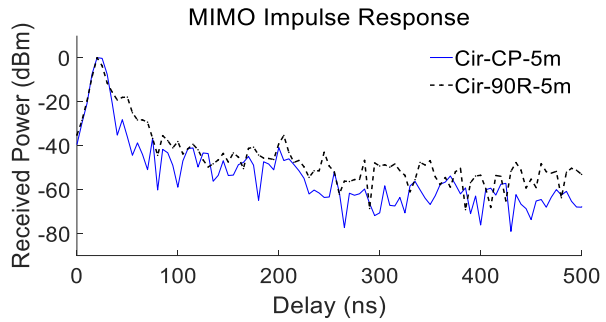

Fig. 3. MIMO-B2B normalized impulse responses for the Cir-CP and Cir-90R setups at the LOS' 5 m distance.

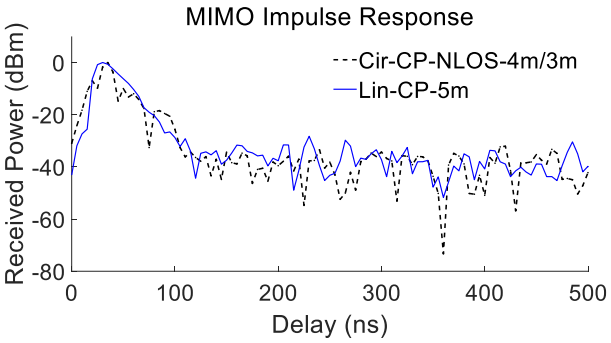

Fig. 4. MIMO-B2B normalized impulse responses for the Cir-CP setup at NLOS and Lin-CP setup at LOS for a distance of 5 m.

time, some of the MPCs are filtered due to a change in the handedness nature of the reflected signal [22]. Regarding the NLOS situation, it is clear that the Cir-CP-NLOS impulse response exhibits a dominant MPC and other smaller less significant MPCs; in addition, this configuration is the most abundant in deep fades. Comparing the Cir-CP with the Lin-CP, it is noticed that the linear setup receives somewhat higher multipath powers. This is due to the fact that the linear setup is able to effectively receive reflected signals from the mine walls and body surfaces. These multipath signals reach the receiver at different phase shifts and often add in a destructive manner, as it shall be seen from the PL results.

B. Path Loss

The PL is defined as the ratio of the transmitted power and a local average of the received power, and is usually computed using the following formula [7]:

$$\mathrm{PL_{dB}} = 20\mathrm{Log}_{10}(\xi\{\mathrm{H_{x,y,f}}\}) \tag{2}$$

where $\mathrm{PL_{dB}}$ is the PL at a certain position, $\mathrm{H_{x,y,f}}$ is the spatial subchannel path strength at a given frequency, and ξ is the averaging operator over all Rx antennas, Tx antennas, frequencies, and snapshots [7].

Usually, the PL is modeled as a function of the Tx-Rx distance d as follows [21]:

$$PL(d) = PL_{dB}(d_0) + 10.\alpha \cdot log_{10}\left(\frac{d}{d_0}\right) + X \tag{3}$$

where $PL_{dB}(d_0)$ represents the mean PL at the reference distance d_0, $10 \cdot \alpha \cdot log_{10}(d/d_0)$ is the mean PL referenced

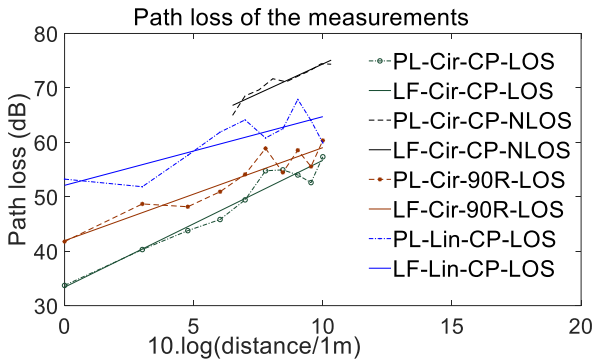

Fig. 5. Cir and Lin polarizations' PL and linear fitting at the MIMO-CP and MIMO-90R scenarios for LOS and NLOS configurations.

to d_0, d is the distance between the Tx and Rx, α is the PL exponent, and X is a zero mean Gaussian variable (in dB) representing shadowing [21].

PL as a function of distance, for different MIMO-B2B scenarios, is shown in Fig. 5. The mean PL and the PL exponent α were determined through the least square regression analysis. The shadowing (X)' standard deviation is designated by the Greek letter σ.

From the PL results, it is noticed that the Cir-CP-LOS' B2B channel performs best with regard to the PL values (the lowest of all configurations), followed closely by the Cir-90R-LOS. The cross-polarization does not affect much the PL results since the circularly polarized antennas are able to receive the signal in both the horizontal and vertical planes. Comparing the linear and the circular polarizations, it is noticed that the circular polarization (Cir-CP) performs better than the linear polarization (Lin-CP) in terms of PL values but not in terms of PL exponents. It seems that the wave reflections from the body surfaces and surrounding objects (shifted in phase compared to the original wave) often add destructively to the received signal. This is clearly explained by the two-ray model in [13] where the reflected wave is demonstrated to be 180° out of phase compared to the incident wave for small values of the incident angle (i.e., grazing incidence) and a perfect reflection (conductive surface). Regarding the circular polarization, which effectively suppresses the first reflection [22], the destructive combining of the reflected signal (especially the first and third reflections) with the LOS signal is not possible. In fact, these reflected waves have opposite handedness making it undetectable in the reception. It was observed that the PL exponent is smaller than the free-space PL exponent (which is equal to 2) for the Cir-XP-LOS and the Lin-CP-LOS configurations due to the waveguide effect of the mine tunnel. The effect of an obstructed line of sight is characterized by a significant increase in PL for the Cir-CP-NLOS compared to the Cir-CP-LOS (about 30 dB increase at the 5 m distance). Moreover, the presence of mining machinery in the vicinity of a short-range B2B link often leads to shadowing and scattering that affect the PL results. As expected, while the mean shadowing is close to zero for all situations, the STD of the shadowing (σ) shows a wider variability of the received signal with respect to the theoretical

TABLE III
PL EXPONENT VALUES FOR DIFFERENT CHANNEL CONFIGURATIONS

Polarization	**Circular**			**Linear**
Parameters	CP-LOS	90R-LOS	CP-NLOS	CP
PL-exponent	2.33	1.71	2.18	1.26
RMSE (dB)	1.84	2.10	1.01	3.10
Shadowing-STD σ (dB)	1.73	1.98	0.946	2.92
Shadowing-Mean (dB)	-0.0038	-0.0036	-0.0035	-0.0018

linear approximation at the LOS situations. This is due to the time variation of signal power at the receiver caused by the changes in the transmission path, which is referred to as fading. Different MPCs sometimes add constructively and in other times destructively leading to the variations of PL around the mean as shown in Fig. 5. It should be noticed that at NLOS, the presence of a mining machine causes a strong reflection which dominates the other multipath arriving by diffraction and rough-wall reflections. In LOS, there are two strong signals arriving at the receiver, namely the LOS signal and the reflection from a close by mining machine. The creeping wave arriving to the receiver from the body surface is not a significant contributor, since the patch antenna does not effectively receive a signal parallel to the plane of the antenna. From the RMSE results in Table III, it is observed that the straight-line PL model is a good approximation of the PL results.

C. Spatial Correlation Matrices

The spatial correlation matrix consists of the correlation coefficients among the subchannels of the MIMO system. It is reported that the presence of a strong ray increases correlation among the subchannels [7], [23]. The correlation coefficient between subchannels h_{AB} and h_{CD} is represented by [7], [23]

$$\rho_{AB}^{CD} = \frac{cov(h_{AB}, h_{CD})}{\sigma_{AB} \times \sigma_{CD}} \tag{4}$$

where $cov(.)$ is the covariance operator and σ_{AB} and σ_{CD} represent the standard deviations of the complex signals h_{AB} and h_{CD}, respectively.

The spatial correlation matrix of the 2×2 MIMO-B2B channel, which we name $\mathbf{R}$, can be written as [24]

$$\mathbf{R} = \begin{bmatrix} 1 & \rho_{11}^{12} & \rho_{11}^{21} & \rho_{11}^{22} \\ \rho_{12}^{11} & 1 & \rho_{12}^{21} & \rho_{12}^{22} \\ \rho_{21}^{11} & \rho_{21}^{12} & 1 & \rho_{21}^{22} \\ \rho_{22}^{11} & \rho_{22}^{12} & \rho_{22}^{21} & 1 \end{bmatrix} \tag{5}$$

TABLE IV
CORRELATION MATRICES FOR DIFFERENT SETUPS AT THE 5 m DISTANCE

Cir-CP-LOS

$$\begin{bmatrix} 1 & 0.46-0.51i & 0.39-0.37i & 0.35-0.44i \\ 0.46+0.51i & 1 & 0.8674 & 0.83-0.07i \\ 0.39+0.37i & 0.8674 & 1 & 0.92+0.04i \\ 0.35+0.44i & 0.83+0.07i & 0.92-0.04i & 1 \end{bmatrix}$$

Cir-90R-LOS

$$\begin{bmatrix} 1 & 0.84-0.06i & 0.44-0.51i & 0.53-0.66i \\ 0.84+0.06i & 1 & 0.59-0.36i & 0.64-0.64i \\ 0.44+0.51i & 0.59+0.36i & 1 & 0.73 \\ 0.53+0.66i & 0.64+0.64i & 0.73 & 1 \end{bmatrix}$$

Cir-CP-NLOS

$$\begin{bmatrix} 1 & 0.11-0.18i & 0.31-0.21i & 0.02-0.16i \\ 0.11-0.18i & 1 & 0.26-0.22i & 0.271-0.13i \\ 0.31-0.21i & 0.26-0.22i & 1 & 0.34-0.13i \\ 0.02-0.16i & 0.271-0.13i & 0.34-0.13i & 1 \end{bmatrix}$$

Lin-CP-LOS

$$\begin{bmatrix} 1 & 0.06-0.46i & 0.59-0.41i & 0.72-0.13i \\ 0.06-0.46i & 1 & -0.25-0.45i & 0.04-0.49i \\ 0.59-0.41i & -0.25-0.45i & 1 & 0.69-0.30i \\ 0.72-0.13i & 0.04-0.49i & 0.69-0.30i & 1 \end{bmatrix}$$

TABLE V
CORRELATION BETWEEN TWO TRANSMITTED SIGNALS AT A CERTAIN RX ANTENNA AND CORRELATION BETWEEN TWO RECEIVED SIGNALS FOR A CERTAIN TX ANTENNA AT THE 5 m DISTANCE

	Correlation between transmitted signals		Correlation between received signals	
	$\lvert\rho_{11}^{12}\rvert$	$\lvert\rho_{21}^{22}\rvert$	$\lvert\rho_{11}^{21}\rvert$	$\lvert\rho_{22}^{12}\rvert$
Cir-CP-LOS	0.68	0.92	0.54	0.84
Cir-XP-LOS	0.69	0.73	0.68	0.85
Cir-CP-NLOS	0.21	0.37	0.37	0.30
Lin-CP-LOS	0.46	0.75	0.72	0.49

where ρ_{AB}^{CD} is the correlation coefficient between subchannels h_{AB} and h_{CD} as represented in (4).

The spatial correlation matrices of the 2×2 B2B-MIMO channels are derived using (5) and represented in Table IV.

A well-established method for the evaluation of MIMO-B2B performance is to compare the transmit and the receive correlation [7]. From the spatial correlation matrices, the transmit correlation (between the two Tx signals) is determined. It is equal to ρ_{11}^{12} at Rx antenna 1 and ρ_{21}^{22} at Rx antenna 2. Similarly, the receive correlation (between two received signal) is determined assuming the signal transmitted from Tx antenna 1 as ρ_{11}^{21}, and assuming the signal transmitted from Tx antenna 2 as ρ_{22}^{12}. The modulus operator $(|\cdot|)$ is used to get easily comparable values as in [23].

From the results in Table V, it is clear that at LOS situations, both the transmit and the receive correlations are significant,

especially for the circularly polarized setup. The linearly polarized MIMO-B2B channel reflects somewhat less correlation than the circularly polarized setup in most situations. This is due to the fact that the fading for the two signals received by the Cir setup (which rejects much of the first reflection power) is somewhat less independent than those received by the Lin setup, due to the presence of a stronger LOS component in the case of the Cir setup. It is important to note that both the Tx and Rx surrounding environments are rich in scattering objects and reflection mediums. Hence, both the receive and transmit correlations are close in values. Moreover, it is observed that the transmit correlation at Rx antenna 1 and the receive correlation at Tx antenna 1 are lower than those corresponding to the Rx antenna 2 and Tx antenna 2, respectively. This is due to the fact that position 1 for both the transmitter and the receiver is closer to the scattering objects than position 2. We conclude that at LOS situations, the half wavelength separations between Tx and Rx do not grantee a low level of correlation as seen in [25]. With regard to the NLOS situation, expectedly, the transmit and receive correlations are considerably lower than the corresponding LOS ones, due to the significantly lower dominant MPC and to the rich scattering phenomenon.

D. RMS Delay Spread and Coherence Bandwidth

The root mean square (rms) delay spread is equal to the square root of the second central moment of the PDP [13] and is derived using the following formula [13]:

$$\tau_{RMS} = \sqrt{\overline{\tau}^2 - \bar{\tau}^2} \tag{6}$$

where $\overline{\tau^2}$ represents the second moment of the PDP and $\bar{\tau}$ denotes the mean excess delay, which is expressed as follows [13]:

$$\overline{\tau} = \frac{\sum_k p(t_k) t_k}{\sum_k p(t_k)} \tag{7}$$

where $p(t_k)$ denotes the power of the kth path and t_k its corresponding delay.

The coherence bandwidth (B_c) is derived from the rms delay spread (for a frequency correlation function above 0.5) as follows [13]:

$$B_c \simeq \frac{1}{5\tau_{RMS}}. \tag{8}$$

The rms delay spread and coherence bandwidth have been computed for each measured PDP of the MIMO-B2B channels under different scenarios of Table I. From Fig. 6, it is observed that for the LOS topologies, the rms delay spreads and coherence bandwidth does not have a monotonic trend with distance. This is due to the fact that the multipath richness is not necessarily increasing with distance, as clearly demonstrated by the K-factor results in Section III-E. The linear setup exhibits higher rms delay spread than the circular setup, and the NLOS setup exhibits higher rms delay spread than its LOS counterpart. This is due to the fact that the circular setup suppresses the first reflection because of a change in the handedness nature of the reflected signal compared to the original signal. These secondary reflections are not totally suppressed due to the surface roughness caused depolarization [26] but they are greatly reduced in strength. With regard to the coherence bandwidth, it has the opposite behavior of the rms delay spread due to the inverse proportionality of the two parameters. In general, the Cir-CP-LOS setup exhibits the best time dispersion results (with rms delay spreads ranging from 8.1 to 19.8 ns) followed closely by the Cir-XP-LOS.

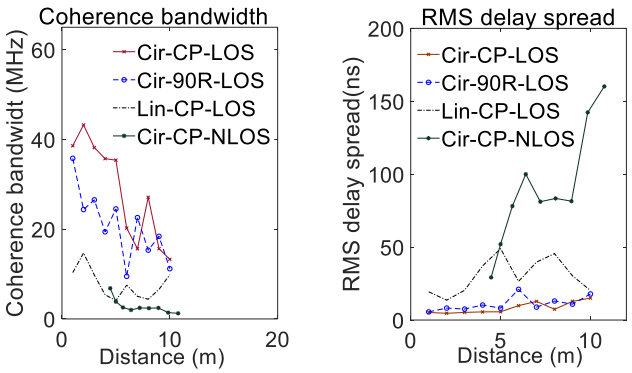

Fig. 6. Rms delay spread and coherence bandwidth, compared for Cir versus Lin polarizations, MIMO-CP versus MIMO 90R scenarios, and LOS versus NLOS.

E. Rican K-Factor

The Rician K-factor is defined as [27]

$$K = \frac{P_D}{2P_R} \tag{9}$$

where P_D corresponds to the power of the dominant component and $2P_R$ is the power of the reflected, diffracted, or diffusely scattered components.

It is directly determined from the impulse response as [27]

$$K = \frac{|V_D|^2}{\sum_{m=1}^{M} |a_m|^2} \tag{10}$$

where M is the number of MPCs, a_m is the random amplitude of the MPC, and V_D is the amplitude of the dominant component (usually equaling the deterministic LOS component).

Since the measurements involved LOS and NLOS situations for different path lengths, the K-factor (denoted in Fig. 7) varied depending on the studied situation and the Tx-Rx distance. The K-factors for the LOS links are clearly higher than that of an NLOS link due to the strong dominant components at LOS. With regard to the effect of polarization, it is shown that the K-factor for the Lin-MIMO setup is generally lower than that of the circularly polarized setup due to the effective rejection of some significant MPCs by the circular antennas. In fact, it is emphasized by the impulse response results (see Figs. 3 and 4) that the MPC powers (relative to the dominant power) are more significant in the case of the Lin-MIMO setup. These MPCs experience different phase shifts, which often lead to destructive power combination at the receiver, as previously demonstrated by the PL results. It is noticed that the Rician K-factor generally reflects the opposite behavior of the rms delay spread. This could be explained by the fact that the rms delay spread generally increases with

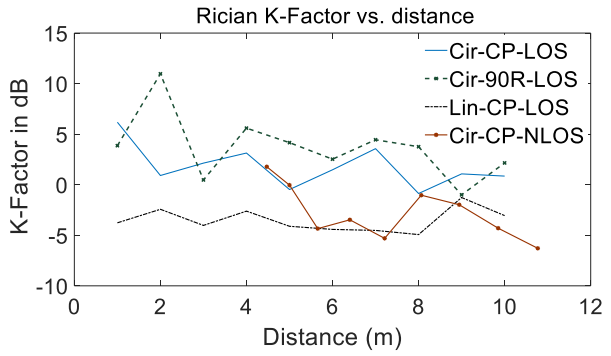

Fig. 7. Rican K-factor for the B2B channels.

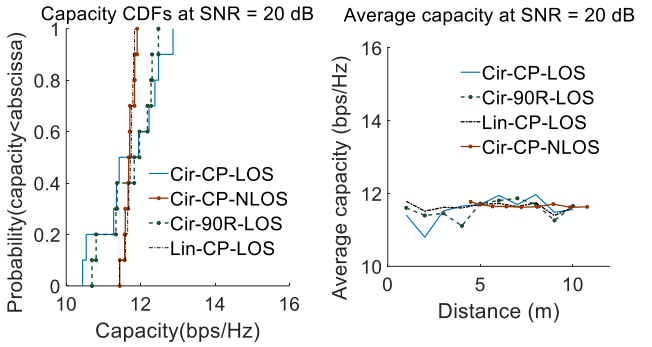

Fig. 8. Cir and Lin polarizations' MIMO channel average capacities and capacity CDFs (for a 5 m distance) at the CP and 90R scenarios, assuming a fixed SNR of 20 dB.

the increase of MPCs richness. A more precise relationship between the K-factor and the rms delay spread was proposed by Witrisal *et al.* [28]. Moreover, it is observed that a higher Rician K-factor corresponds to a higher correlation. This is due to the direct effect of scattering (which enriches multipath) in lowering both the correlation as well as the K-factor.

F. Channel Capacity

The aim of the capacity study is to show the effect of the PL—on the one hand—and that of the multipath—on the other hand—on the different MIMO-B2B channels. This is achieved by assuming a constant transmitted power and variable SNR in the first case and by assuming a fixed SNR in the second case [21].

The MIMO channel capacity is derived using the following formula [21]:

$$C_{MIMO}[bps/Hz] = log_2(\det[\boldsymbol{I}_n + \frac{SNR_{av}}{m}\boldsymbol{H}\boldsymbol{H}^*]) \quad (11)$$

where $\boldsymbol{I}_n$ is the identity matrix, SNR_{av} is the average SNR, H is the normalized $m \times n$ channel response, and * signifies the complex conjugate transpose operator.

1) Capacity at a Constant SNR: When fixing the SNR value, the PL is isolated from the capacity calculations [21]. Hence, this article allows analyzing the effect of the multipath on the MIMO-B2B capacity.

Fig. 8 represents the channel capacity results at an SNR of 20 dB for the different MIMO-B2B configurations. From the average capacities and the capacity cumulative distribution functions (CDFs), it is clear that the circular setup exhibits higher fluctuations in the channel capacity when changing the distance and at different snapshots for the same distance. This is due to the roughness of the walls which affect the first reflection depolarization [26] and, hence, its contribution to channel capacity. As expected, in the lower distances, the circular setup was not able to effectively receive enough multipath power and exhibited lower capacity values. This is due to the fact that, at the lower distances, the main multipath power is generated by the body parts' reflections rather than the reflection and diffraction from the relatively distant mine walls. The body, being a smooth surface, causes the signal handedness to change and the reflection is effectively suppressed at the reception. Moreover, it is observed that the channel capacity, at a constant SNR, is somewhat stable for the linear setup and the Cir-NLOS setup. This is due to the fact that a linear setup receives multipath contributions from the reflections of both the body and mine walls. Moreover, reflections of the mine walls are the main contributors to the Cir-NLOS multipath richness. The availability of these reflections is somewhat stable for the measurement distances.

TABLE VI

THROUGHPUT GAIN FOR THE B2B CHANNELS WHEN SNR = 20 dB

Channel	Throughput gain
Cir-CP-LOS	1.738
Cir-90R-LOS	1.736
Cir-CP-NLOS	1.752
Lin-CP-LOS	1.748

In addition, the improvement in channel capacity offered by MIMO over the corresponding SISO link is studied. As expected, the throughput gain, which quantifies this improvement, is shown to be highest for the Cap-Cir-CP-NLOS channel followed by the Cap-Lin-CP-LOS channel due to their small correlation values. Moreover, throughput gains (summarized in Table VI) are found to be less than 2 for all the B2B channels due to correlation.

2) Capacity at a Constant Transmit Power: At a constant transmit power of −10 dBm, the channel capacity was computed for different MIMO-B2B configurations. In this article, both the multipath richness and the PL have an effect on the channel capacity. Fig. 9 shows the derived results for the MIMO configuration.

As expected, the channel capacity results—when a constant transmitted power is considered—show that the average channel capacity decreases with distance. In fact, the smaller distances correspond to higher received average powers and, hence, higher average SNRs which has a direct impact on the capacity as denoted in (11). Comparing the MIMO-Cir-CP-LOS with the MIMO-Lin-CP-LOS' B2B channels, it is clear that the circular setup outperforms the linear one, beside the fact that the multipath richness is actually higher when using the linear setup. This is due to the destructive combination of the MPCs, resulting in a lower total received power for the Lin setup. In fact, some reflected signals are out of phase compared to the incident wave as explained in the PL section. In some distances, however, a constructive combining

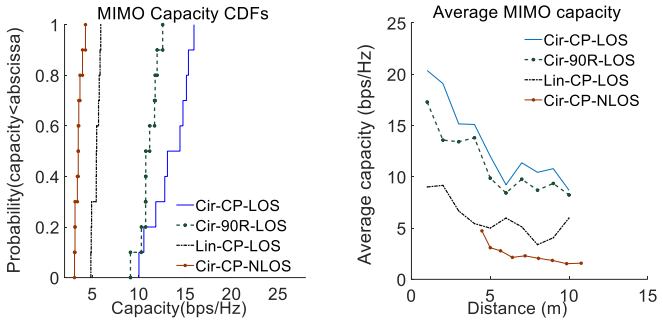

Fig. 9. Circular and linear polarizations' MIMO average channel capacities and capacity CDFs (for a 5 m distance) at the CP and 90R scenarios and a constant transmit power.

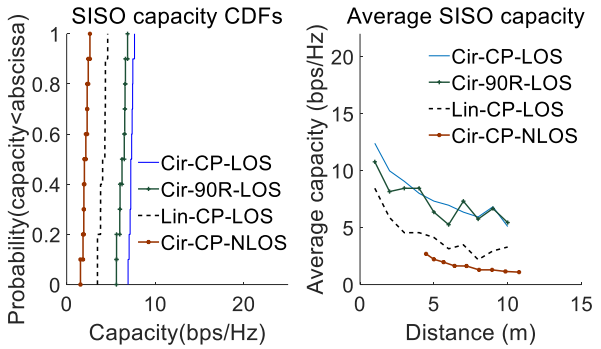

Fig. 10. Circular and linear polarizations' SISO average channel capacities and capacity CDFs (for a 5 m distance) at the CP and 90R scenarios and a constant transmit power.

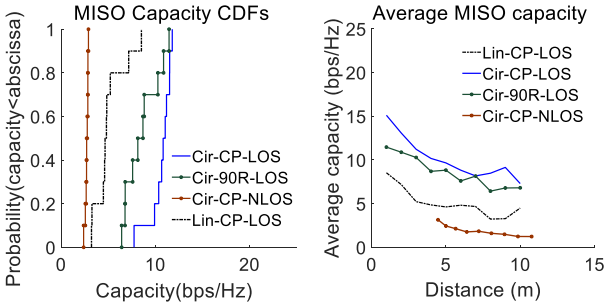

Fig. 11. Circular and linear polarizations' MISO average channel capacities and capacity CDFs at the CP and 90R scenarios and a constant transmit power.

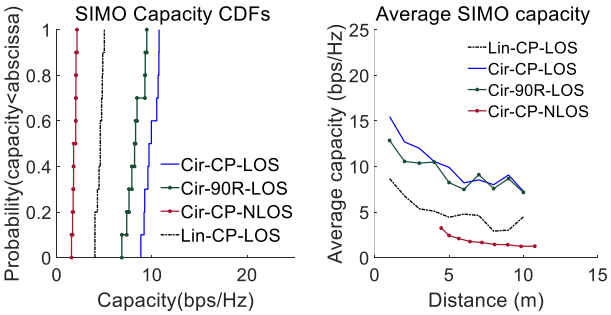

Fig. 12. Circular and linear polarizations' SIMO average channel capacities and capacity CDFs at the CP and 90R scenarios and a constant transmit power.

of the MPCs occurs, which explains the relative increase in the channel capacity for the linear setup at these distances (2, 6, 9, and 10 m). This result is also observed in the PL graph, where the PL values for the Lin-CP-LOS are below the linear approximation due to the constructive MPCs combining at these distances. Concerning the circular setup, both the CP and 90R configurations exhibit close results. Comparing the Cir-CP-LOS to the Cir-CP-NLOS, it is clear that the LOS topology exhibits a considerably higher capacity due to the lower PL at the LOS scenario. It is noticed that the capacity CDFs (for a 5 m distance) confirm the same results observed from the average capacity graphs. Moreover, these CDFs show a greater variation (between 10 and 15 bps/Hz) for the measured capacities of the Cir-CP-LOS at different snapshots compared to other scenarios. It seems that the reflected signals from the walls are depolarized in different ways; each time a snapshot is taken due to the random roughness of the walls which receive the signals at considerably different angles at each snapshot. Hence, sometimes, the first reflection is suppressed mostly, and sometimes, some power of this reflection is available due to depolarization from the rough surface and adds as a power contribution at the receiver.

A comparison of the MIMO capacity results with their corresponding MISO presented in Fig. 11, SIMO denoted in Fig. 12, and SISO denoted in Fig. 10 results shows a considerable improvement of the channel capacity, despite the relatively strong correlation among the subchannels, especially at LOS. Moreover, it is observed that MISO systems perform worse than the SIMO in terms of throughput gain (improvement relative to SISO). For instance, it is calculated for the Cir-CP scenarios—at the 5 m distance and a constant transmitted power—to be 1.66 for MIMO, 1.37 for SIMO, and 1.32 for MISO. It is less than 2 for the MIMO scenario because of the considerable correlation at both the transmission and the reception. In addition, since the receive correlation is somewhat less than the transmit correlation, the SIMO throughput gain is slightly higher in the case of SIMO as was also noticed in several WBAN publications [24].

Hence, the circular polarization combined with MIMO proved to be a viable solution for the B2B communication inside a mine.

G. Channel Modeling

The modeling procedure consists in developing the impulse response to describe the B2B system in a mining environment. The latest, which completely characterizes the B2B channel, is represented as follows [15]:

$$h(t) = \sum_{i=0}^{N-1} a_i \delta(t - t_i) e^{j\theta_i} \tag{12}$$

where N is the number of MPCs, and a_i, t_i, and θ_i are, respectively, the random amplitude, arrival time, and phase of the i^{th} MPC. δ is the Kronecker delta function.

The modeling procedure consists of two steps, namely the path amplitudes (a_i) and arrival times (t_i) modeling. This is done by expressing the path amplitudes as random Gaussian variable with average powers decaying exponentially, as represented by the IEEE 802.11 Channel Model [14]. The arrival times are modeled by comparing them with different distributions used in the literature. The phases are assumed

to be statistically independent random variables, uniformly distributed from 0 to 2π [15]. The modeled impulse response shall approximate the measurements-based impulse response for the studied B2B channel.

1) Path Amplitude Modeling: One of the most popular indoor channel models is the exponential model where power decreases exponentially with the channel delay [14]. Based on the exponential model, the IEEE 802.11b Task Group has created a model, where the channel impulse response is represented by the output of the finite impulse response filter. The different channel taps (representing the MPCs) are modeled by independent complex Gaussian random variables with average powers that follow the exponential PDP [14].

The power of each channel tap is given by [14]

$$P_i^2 = P_0^2 * e^{-i*T_s/\sigma_\tau} \tag{13}$$

where i is the tap index (between 0 and N), T_s is the sampling time, σ_τ is the rms delay spread, and P_0^2 is the power of the first tap determined in such a way to make the average received power equal to one, as follows:

$$P_0^2 = \frac{1 - e^{-T_s/\sigma_\tau}}{1 - e^{-(N+1)T_s/\sigma_\tau}}. \tag{14}$$

The modeling of the path amplitudes described by (13) and (14) requires the knowledge of the rms delay spread. This latest could either be determined empirically from measurements or estimated from published results in similar environments. In our case, we have used the rms delay spread that was calculated from our SISO-B2B measurements at the chosen 6 m distance as 12 ns.

2) Time of Arrival Modeling: The time of arrival of the different MPCs is derived from the measurements by applying a peak detection algorithm on the measured PDP. The time difference between successive peaks is considered in order to generate a random set for our process; in fact, the mere time of arrival is not completely random since it is always increasing. The distribution of the arrival times' steps is compared to the different random distributions from the literature, namely, Poisson, Gaussian, and Weibull. Kolmogorov–Smirnov (KS) test is used to determine the distribution that most closely describes the random set of time steps. Results in Fig. 13 show that the Poisson distribution offers the best fit for these time steps, followed closely by the Weibull distribution. The supremum of the set of distances (differences between the measurements and model CDFs) for the Poisson, Weibull, and Gaussian is 0.224, 0.225, and 0.269, respectively. The time differences between peaks of the MPCs can now be generated using a random vector following the optimal distribution. The first time of arrival is nothing more than that of the LOS signal denoted by the well-known formula

$$\mathrm{T} = \mathrm{D}/\mathrm{V} \tag{15}$$

where V is the wave velocity (empirically estimated from a set of measured PDPs to be 0.9 *C, where C is the speed of light) and D is the measurements' distance. Finally, the time of arrival is determined by adding the individual time steps from the random vector to their corresponding arrival times.

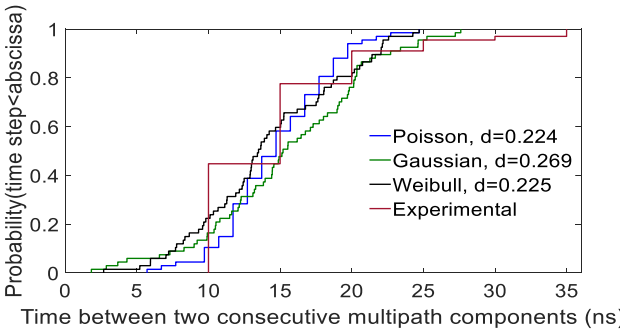

Fig. 13. Comparison of three optimal CDFs to represent the time differences between MPCs.

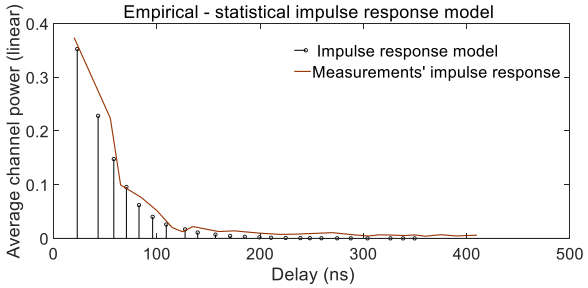

Fig. 14. Modeled versus measured impulse responses normalized by their respective total powers.

For instance, the first arrival time added to the first time step will give the second time of arrival.

The impulse response is readily determined by matching the arrival times to the path amplitudes as denoted in Fig. 14. In order to compare the modeled and measured impulse responses, the measured impulse response was also determined so as to make the average received power equal to one. This is done by dividing the received power over the sum of all the MPC powers. The modeled impulse response is found to be close to the measured one with a calculated mmse of 1.8437e−04.

IV. Conclusion

In this article, the MIMO-B2B channel was characterized at 2.4 GHz in a mine gallery using circularly and linearly polarized antennas. Different scenarios were considered, namely CP and 90R at LOS and NLOS. It is clear from the PL, capacity, and time dispersion results that the circularly polarized antennas perform best for B2B channels in a mine environment due to their resilience to antennas misalignments. The channel capacities are strongly dependent upon PL as well as the multipath richness at a lower degree. Hence, as the multipath richness becomes significant at the higher distances, the channel capacities experience an occasional increase despite the PL effect. K-factor results reveal that the MPC powers relative to the dominant power are more significant in the case of the Lin-MIMO setup than the Cir-MIMO setup. The rms delay spread shows this result with higher values for Lin-CP, especially at higher distances. Correlation follows the same trend as the K-factor due to the effect of scattering in lowering both the correlation as well as the K-factor. The effect of an obstructed

LOS signal is significant as seen from the PL, capacity, and time dispersion results. In fact, the Cir-CP-NLOS capacities are lower than half of the Cir-CP-LOS capacities at similar Tx-Rx separations. This is expected, since the LOS is the main contributor to the total power, added to the fact that the second contribution (the first reflection) is not effectively received at the receiver, due to the relative change of handedness of the reflected circularly polarized signal. The MIMO throughput gain is most significant for the NLOS setup as well as the linear setup because of their low branch correlation. In general, the circularly polarized setup seems to be very well suited for the B2B propagation inside a mine, even at NLOS.

An impulse response model has been developed in order to completely describe the B2B channel. The Poisson distribution best describes the path arrival time steps. The path amplitudes are modeled using the exponential model that assumes that the MPCs amplitudes follow a Gaussian distribution while their average powers follow an exponentially decaying PDP.

REFERENCES

[1] M. El Azhari, M. Nedil, I. B. Mabrouk, L. Talbi, K. Ghanem, and Y. S. Alj, "Performance evaluation of a MIMO-on-body system in a mine environment," *Prog. Electromagn. Res. C*, vol. 61, pp. 55–63, 2016.

[2] Y. Rissafi, L. Talbi, and M. Ghaddar, "Experimental characterization of an UWB propagation channel in underground mines," *IEEE Trans. Antennas Propag.*, vol. 60, no. 1, pp. 240–246, Jan. 2012.

[3] A. Benzakour, S. Affes, C. Despins, and P.-M. Tardif, "Wideband measurements of channel characteristics at 2.4 and 5.8 GHz in underground mining environments," in *Proc. Veh. Technol. Conf.*, Sep. 2004, pp. 3595–3599.

[4] C. Briso-Rodriguez, J. M. Cruz, and J. I. Alonso, "Measurements and modeling of distributed antenna systems in railway tunnels," *IEEE Trans. Veh. Technol.*, vol. 56, no. 5, pp. 2870–2879, Sep. 2007.

[5] K. Guan, Z. Zhong, J. I. Alonso, and C. Briso-Rodriguez, "Measurement of distributed antenna systems at 2.4 GHz in a realistic subway tunnel environment," *IEEE Trans. Veh. Technol.*, vol. 61, no. 2, pp. 834–837, Feb. 2012.

[6] G. R. Valenzuela, "Depolarization of EM waves by slightly rough surfaces," *IEEE Trans. Antennas Propag.*, vol. AP-15, no. 4, pp. 552–557, Jul. 1967.

[7] I. Ben Mabrouk, L. Talbi, M. Nedil, and K. Hettak, "MIMO-UWB channel characterization within an underground mine gallery," *IEEE Trans. Antennas Propag.*, vol. 60, no. 10, pp. 4866–4874, Oct. 2012.

[8] B. Mnasri, M. Nedil, N. Kandil, M. Ghaddar, and L. Talbi, "Experimental investigation of 2.4 GHz MIMO channel capacity using 4×4 butler matrix in underground mine gallery," *IEEE Trans. Antennas Propag.*, to be published.

[9] I. Mabrouk, L. Talbi, M. Nedil, Y. Coulibaly, and T. Denidni, "Effect of antenna directivity on performance of multiple input multiple output systems in an underground gold mine," *IET Microw., Antennas Propag.*, vol. 6, no. 5, pp. 555–561, Apr. 2012.

[10] M. E. Azhari, M. Nedil, I. Ben Mabrouk, and L. Talbi, "Multipath effect on off-body channel parameters of a MIMO system using patch antennas inside a mine," in *Proc. IEEE Int. Symp. Antennas Propag. (APSURSI)*, Fajardo, Puerto Rico, Jun. 2016, pp. 1693–1694.

[11] M. E. Azhari, M. Nedil, I. Ben Mabrouk, and L. Talbi, "Path loss effect on off-body channel capacity of a MIMO system using patch antennas inside a mine," in *Proc. IEEE Int. Symp. Antennas Propag. (APSURSI)*, Fajardo, Puerto Rico, Jun. 2016, pp. 1697–1698.

[12] E. Reusens *et al.*, "Characterization of on-body communication channel and energy efficient topology design for wireless body area networks," *IEEE Trans. Inf. Technol. Biomed.*, vol. 13, no. 6, pp. 933–945, Nov. 2009.

[13] T. S. Rappaport, *Wireless Communications: Principles and Practice*, 2nd ed. Upper Saddle River, NJ, USA: Prentice-Hall, 2002.

[14] M. El Hassan El Azhari, L. Talbi, L. Arabi, M. Nedil, M. L. Seddiki, and N. Kandil, "Channel characterization of circularly polarized antenna MIMO system in an underground mine," *Prog. Electromagn. Res. M*, vol. 67, pp. 9–19, 2018.

[15] J. Ryckaert, P. De Doncker, R. Meys, A. De Le Hoye, and S. Donnay, "Channel model for wireless communication around human body," *Electron. Lett.*, vol. 40, no. 9, pp. 543–544, Apr. 2004.

[16] A. E. Forooshani, S. Bashir, D. G. Michelson, and S. Noghanian, "A survey of wireless communications and propagation modeling in underground mines," *IEEE Commun. Surveys Tuts.*, vol. 15, no. 4, pp. 1524–1545, 4th Quart., 2013.

[17] Y. S. Cho, J. Kim, W. Y. Yang, and C. G. Kang, *MIMO-OFDM Wireless Communications With MATLAB*. Hoboken, NJ, USA: Wiley, 2010.

[18] M. Boutin, A. Benzakour, C. L. Despins, and S. Affes, "Radio wave characterization and modeling in underground mine tunnels," *IEEE Trans. Antennas Propag.*, vol. 56, no. 2, pp. 540–549, Feb. 2008.

[19] F. A. Dicandia, S. Genovesi, and A. Monorchio, "Analysis of the performance enhancement of MIMO systems employing circular polarization," *IEEE Trans. Antennas Propag.*, vol. 65, no. 9, pp. 4824–4835, Sep. 2017.

[20] J. Wang, Z. Lv, and X. Li, "Analysis of MIMO diversity improvement using circular polarized antenna," *Int. J. Antennas Propag.*, vol. 2014, pp. 1–9, 2014.

[21] M. El Azhari, M. Nedil, I. B. Mabrouk, K. Ghanem, and L. Talbi, "Characterization of an off-body channel at 2.45 GHZ in an underground mine environment," *Prog. Electromagn. Res. M*, vol. 43, pp. 91–100, 2015.

[22] J. D. Jackson, *Classical Electrodynamics*, 3rd ed. New York, NY, USA: Wiley, 1998.

[23] R. E. Jaramillo, O. Fernandez, and R. P. Torres, "Empirical analysis of a 2×2 MIMO channel in outdoor-indoor scenarios for BFWA applications," *IEEE Antennas Propag. Mag.*, vol. 48, no. 6, pp. 57–69, Dec. 2006.

[24] I. Khan and P. Hall, "Experimental evaluation of MIMO capacity and correlation for narrowband body-centric wireless channels," *IEEE Trans. Antennas Propag.*, vol. 58, no. 1, pp. 195–202, Jan. 2010.

[25] J. Colburn, Y. Rahmat-Samii, M. Jensen, and G. Pottie, "Evaluation of personal communications dual-antenna handset diversity performance," *IEEE Trans. Veh. Technol.*, vol. 47, no. 3, pp. 737–746, Aug. 1998.

[26] S.-C. Kwon and G. L. Stuber, "Geometrical theory of channel depolarization," *IEEE Trans. Veh. Technol.*, vol. 60, no. 8, pp. 3542–3556, Oct. 2011.

[27] P. Tang, J. Zhang, A. F. Molisch, P. J. Smith, M. Shafi, and L. Tian, "Estimation of the K-factor for temporal fading from single-snapshot wideband measurements," *IEEE Trans. Veh. Technol.*, to be published, doi: 10.1109/TVT.2018.2878352.

[28] K. Witrisal, Y.-H. Kim, and R. Prasad, "A new method to measure parameters of frequency-selective radio channels using power measurements," *IEEE Trans. Commun.*, vol. 49, no. 10, pp. 1788–1800, Oct. 2001.

Moulay El Hassan El Azhari received the bachelor's and master's degrees in electrical and electronics engineering from California State University at Sacramento (CSUS), Sacramento, CA, USA, in 2005 and 2008, respectively, and the master's degree in telecommunications engineering from the Université du Québec en Abitibi-Témiscamingue, Val-d'Or, QC, Canada, in 2015. He is currently pursuing the Ph.D. degree with the University of Quebec at Outaouai (UQO), Gatineau, QC, Canada.

He worked as an Electrical Engineer with the Research and Development Department, Motion Control Engineering, Inc., Rancho Cordova, CA, USA, from 2007 to 2011. He has been an Electrical Engineer with the Research and Development Department, Meglab Inc., Val-d'Or, QC, Canada, since 2016. He is also a Researcher with the Telebec Underground Communications Research Laboratory (LRTCS) for the period of 2013–2020. His research interests are in radio-wave propagation for multiple-input–multiple-output systems, measurement campaigns in underground mine environments, and body area networks.

Mr. El Azhari is a member of the Ordre des ingénieurs du Québec. He was awarded the Canadian Natural Sciences and Engineering Research Council (NSERC) Ph.D. Scholarship in 2016.

Larbi Talbi (Senior Member, IEEE) received the M.S. and Ph.D. degrees in electrical engineering from Laval University, Quebec City, QC, Canada, in 1989 and 1994, respectively.

He completed a Post-Doctoral fellowship at the Personal Communications Research Group, INRS-Telecommunications, Montreal, QC, Canada, in 1995, where he led projects supported by Bell Canada, Montreal. From 1995 to 1998, he was an Assistant Professor with the Electronics Engineering Department, Riyadh College of Technology, Riyadh, Saudi Arabia. From 1998 to 1999, he was an Invited Professor with the Electrical and Computer Engineering Department, Laval University. Since 1999, he has been a Professor with the Department of Computer Science and Engineering, University of Quebec at Outaouais, Gatineau, QC, Canada, where he is currently the Ph.D. Program Chair in sciences and information technologies. His research activities include experimental characterization and modeling of UHF/EHF indoor radio propagation channels and the design of antennas and microwave circuits for wireless communication systems. He is actively involved in major projects related to the deployment of wireless technologies in underground mines, mainly experimental characterization of the underground mine channels using multiple-input–multiple-output (MIMO) antennas at 60 GHz, the design of microwave and RF components using SIW technique and metamaterials, and antenna array for wireless applications. He has authored or coauthored more than 170 journal and conference papers.

Dr. Talbi is a member of the Ordre des ingénieurs du Québec.

Mourad Nedil (Senior Member, IEEE) received the Dipl.Ing. degree from the University of Algiers (USTHB), Algiers, Algeria, in 1996, the D.E.A (M.S.) degree from the University of Marne la Vallée, Marne la Vallée, France, in 2000, and the Ph.D. degree from the Institut National de la Recherche Scientifique (INRS-EMT), Université de Québec, Montreal, QC, Canada, in April 2006. He completed a post-doctoral fellowship at the RF Communications Systems Group, INRS-EMT, Montreal, in 2008.

In June 2008, he joined the School of Engineering, Université du Québec en Abitibi-Témiscamingue, Val-d'Or, QC, Canada, where he is currently a Full Professor. His research interests include antennas, multiple-input–multiple-output (MIMO) radio-wave propagation, and microwave devices.